The EMBO Journal (2010) 29, 292–303 | © 2010 European Molecular Biology Organization | All Rights Reserved 0261-4189/10
www.embojournal.org

THE EMBO JOURNAL

ArfGAP1 generates an Arf1 gradient on continuous lipid membranes displaying flat and curved regions

Ernesto Ambroggio[1,4], Benoît Sorre[1,2,4], Patricia Bassereau[2], Bruno Goud[1,*], Jean-Baptiste Manneville[1,*] and Bruno Antonny[3,*]

[1]Laboratoire Mécanismes moléculaires du transport intracellulaire, Institut Curie, CNRS UMR 144, Paris, France, [2]Laboratoire Membranes and Cellular Functions, Institut Curie, CNRS UMR 168, Paris, France and [3]Institut de Pharmacologie Moléculaire et Cellulaire, Université de Nice Sophia Antipolis et CNRS, Valbonne, France

ArfGAP1, which promotes GTP hydrolysis on the small G protein Arf1 on Golgi membranes, interacts preferentially with positively curved membranes through its amphipathic lipid packing sensor (ALPS) motifs. This should influence the distribution of Arf1-GTP when flat and curved regions coexist on a continuous membrane, notably during COPI vesicle budding. To test this, we pulled tubes from giant vesicles using molecular motors or optical tweezers. Arf1-GTP distributed on the giant vesicles and on the tubes, whereas ArfGAP1 bound exclusively to the tubes. Decreasing the tube radius revealed a threshold of $R \approx 35$ nm for the binding of ArfGAP1 ALPS motifs. Mixing catalytic amounts of ArfGAP1 with Arf1-GTP induced a smooth Arf1 gradient along the tube. This reflects that Arf1 molecules leaving the tube on GTP hydrolysis are replaced by new Arf1-GTP molecules diffusing from the giant vesicle. The characteristic length of the gradient is two orders of magnitude larger than a COPI bud, suggesting that Arf1-GTP diffusion can readily compensate for the localized loss of Arf1 during budding and contribute to the stability of the coat until fission.

The EMBO Journal (2010) **29,** 292–303. doi:10.1038/emboj.2009.341; Published online 19 November 2009
Subject Categories: membranes & transport
Keywords: ALPS motif; diffusion; membrane curvature; membrane tube; optical tweezers

Introduction

The spatial and temporal control of the GTP hydrolysis cycle of the small G protein, Arf1, is critical for the proper functioning of the Golgi apparatus (Poon *et al*, 1999; Frigerio *et al*, 2007; Saitoh *et al*, 2009). In its active GTP-bound conformation, Arf1 recruits numerous protein complexes to the Golgi membrane, which all contribute to the transport function of this organelle. This includes coat complexes, which generate transport vesicles, lipid transporters and lipid-modifying enzymes, which control membrane composition, and long coiled-coil proteins, which tether membranes (Gillingham and Munro, 2007).

Two types of GTPase activating proteins (GAPs) for Arf1 exist at the Golgi. Members of the ArfGAP3/Glo3 family target Arf1-GTP in complex with the COPI coat through specific protein–protein interactions (Weimer *et al*, 2008; Kliouchnikov *et al*, 2009; Schindler *et al*, 2009). Members of the ArfGAP1/Gcs1 family seem less dependent on the engagement of Arf1-GTP with specific effectors and instead are mostly regulated by protein–lipid interactions. ArfGAP1 and Gcs1p contain motifs, named amphipathic lipid packing sensor (ALPS), that allow coupling of the GAP activity with the curvature of the underlying membrane (Bigay *et al*, 2005; Mesmin *et al*, 2007; Levi *et al*, 2008). These motifs adsorb specifically at the surface of small artificial liposomes where they form amphipathic helices. As a result of this folding/adsorption mechanism, the rate of ArfGAP1-catalysed GTP hydrolysis on Arf1 increases up to 100-fold when the liposome radius decreases from 150 to 35 nm (Bigay *et al*, 2003).

The hypersensitivity of ArfGAP1 to membrane curvature suggests simple models for the organization of Arf1-driven events at the Golgi apparatus. In the case of COPI vesicles, we proposed that ArfGAP1 gradually eliminates Arf1-GTP molecules from COPI-coated area as the underlying membrane becomes curved. Ultimately, this would result in COPI disassembly once the vesicle has formed (Bigay *et al*, 2003). More recently, we proposed that ArfGAP1 also contributes to the organization of membrane tethering by the long coiled-coil protein GMAP-210 by favouring the connection between flat and curved membranes, a geometry that seems well suited to restrict the movement of vesicles in the vicinity of Golgi cisternae (Drin *et al*, 2008).

All these models were inferred from reconstitution experiments using artificial liposomes made by extrusion through filters of defined pore size. With this technique, one can decrease the mean liposome radius from 150 to 30 nm (Bigay *et al*, 2003). However, such liposomes hardly mimic some complex membrane topologies that are found during budding from Golgi membranes, notably when a transport intermediate is still connected to the parental membrane through a thin neck. The spatial distribution of the GTPase reaction at this stage might be critical for the stability of the coat, the sorting of lipids and cargoes and the susceptibility of the neck to

*Corresponding authors. B Goud or J-B Manneville, Laboratoire Mécanismes moléculaires du transport intracellulaire, Institut Curie, CNRS UMR 144, 26 rue d'Ulm, 75248 Paris Cedex 5, France.
Tel.: +33 1 56 24 6381; Fax : +33 1 56 24 6421;
E-mail: bruno.goud@curie.fr or
Tel.: +33 1 56 24 6417; Fax: +33 1 56 24 6421;
E-mail: Jean-Baptiste.Manneville@curie.fr or B Antonny, Institut de Pharmacologie Moléculaire et Cellulaire, Université de Nice Sophia Antipolis et CNRS, 660 route des lucioles, Valbonne, 06560, France.
Tel.: +33 4 93 95 7775; Fax: +33 4 93 95 7710;
E-mail: antonny@ipmc.cnrs.fr
[4]These authors contributed equally to this work

Received: 11 August 2009; accepted: 23 October 2009; published online: 19 November 2009

undergo fission (Pucadyil and Schmid, 2009). However, these issues are very difficult to address experimentally.

We have developed techniques by which long and thin tubes can be pulled from the membrane of giant unilamellar vesicles (GUVs) (Roux *et al*, 2002; Leduc *et al*, 2004; Sorre *et al*, 2009). These approaches were used here to explore the organization of the GTPase reaction when ArfGAP1 and Arf1-GTP are exposed to a continuous lipid membrane displaying abrupt changes in curvature.

Results

Fluorescent versions of Arf1, of ArfGAP1 and of its ALPS motif region were added to GUVs whose membrane had been mechanically deformed. The protein constructs as well as the nano-techniques used to pull on the GUV membrane have been published (Leduc *et al*, 2004; Mesmin *et al*, 2007; Manneville *et al*, 2008; Sorre *et al*, 2009). In brief, long and thin tubes were pulled from GUVs using either the force of kinesin motors moving along microtubules (Roux *et al*, 2002; Leduc *et al*, 2004) or the force of optical tweezers combined to micropipette aspiration of the GUV (Sorre *et al*, 2009). The first technique is statistically advantageous because numerous tubes are generated in the GUV chamber. The main advantage of the second technique is to allow fine tuning of the tube radius as well as force measurements.

Distribution of Arf1-GTP, ALPS and ArfGAP1 on tube networks

We first generated lipid tubes from GUVs containing DOPC (99%) and the fluorescent lipid Bodipy-TR-Ceramide (BodTRCer; 1%) using kinesin motors. These tubes have a radius of about 20–30 nm as estimated by electron microscopy (Roux *et al*, 2002). The GUV/tube network was then incubated for several minutes with the protein of interest and confocal images were taken either in the equatorial plane of the parental GUVs ('z-GUVs' images) or near the chamber surface to visualize the tubes ('z-tubes' images). In the presence of GTP, myristoylated Arf1, which was labelled at its C-terminus with a green probe (Oregon Green, OG), was found on the tubes as well as on the GUVs (Figure 1A, left panel). To compare the surface density of Arf1 on the two membrane regions, we measured the fluorescent profiles of Arf1-OG (green channel) and of the lipid marker BodTRCer (red channel) along lines perpendicular to the tube main axis or to the GUV membrane (Figure 1A, right panel). The relative surface density of Arf1 in the tube and in the GUV is given by the distribution ratio: $distribution = (\text{Arf1-OG/BodTRCer})_{tube}/(\text{Arf1-OG/BodTRCer})_{GUV}$. The observed value was close to 1.5, suggesting a slight enrichment of Arf1-GTP in the tubular regions. Thus, Arf1-GTP distributes quite evenly at the surface of continuous membranes displaying flat and tubular regions, although a slight preference for tubular regions could be observed.

A strikingly different picture was observed when kinesin-pulled DOPC tubes were exposed to the curvature sensor region of ArfGAP1 (residues 192–304 corresponding to the two ALPS motifs and abbreviated as ALPS1-ALPS2-Alexa^{488}, Figure 1B) or to an antibody-labelled version of ArfGAP1 (Figure 1C). The lipid tubes were strongly labelled by ALPS1-ALPS2-Alexa^{488} or by ArfGAP1, whereas the giant vesicles, from which the tubes depart, displayed no detectable protein labelling. The segregation of ArfGAP1 and of the ALPS1-ALPS2 peptide in the tubes was so high that their fluorescence in the GUVs was similar to background noise precluding the measurement of the distribution ratio, which therefore seemed infinite. These observations show that ArfGAP1, when exposed to a continuous lipid membrane, binds very selectively to high-curvature regions through its ALPS1-ALPS2 region.

Next, we conducted two-stage incubations. The GUV/tube lipid network was first incubated with Arf1-OG and GTP and then with the fluorescent ALPS1-ALPS2 peptide or with antibody-labelled ArfGAP1 (Figure 2A and B, respectively). Again, Arf1-OG was found both on the tubes and on the parental GUVs, whereas ArfGAP1 or the ALPS1-ALPS2 peptide was restricted to the tubes (Figure 2). Of note, antibody-labelled ArfGAP1 did not promote the dissociation of Arf1-OG from the GUV/tube network suggesting that it loses the ability to promote GTP hydrolysis on Arf1. We concluded that ArfGAP1 and its ALPS1-ALPS2 region keep their strict preference for membrane tubes when the entire surface of the GUV/tube network is covered by Arf1-GTP, the substrate of ArfGAP1.

Additional experiments indicated that the interaction of ALPS1-ALPS2 with membrane tubes was reversible. When the incubation chamber containing the GUV/tube network and ALPS1-ALPS2-Alexa^{488} or GTP-bound Arf1-OG was washed out with buffer alone, the ALPS1-ALPS2 signal vanished within a few minutes (Supplementary Figure S1A), whereas the Arf1-OG signal was more stable (Supplementary Figure S1B). In addition, when fluorescent versions of the individual ALPS motifs of ArfGAP1 (ALPS1-Alexa^{488} and ALPS2-Alexa^{488}) were added to GUV/tube networks, almost no signal could be observed (Supplementary Figure S2). Earlier biochemical experiments indicated that each ALPS motif is able to bind to small liposomes, but binding increases 10-fold when the two motifs are in tandem such as in full-length ArfGAP1 (Mesmin *et al*, 2007). This synergy probably explains why DOPC tubes were labelled by the ALPS1-ALPS2 construct but not by the individual motifs.

A curvature threshold for the binding of the ALPS 1-2 motif

The radius of the tubes pulled from GUVs by molecular motors cannot be readily controlled and modified. To circumvent this limitation, we used an alternative approach based on micromanipulation. A GUV in a solution containing the protein of interest was held at a controlled membrane tension by micropipette aspiration. Next, an optically trapped streptavidin-coated bead was adhered to the opposite side of the GUV and a tube was generated by moving the giant vesicle with the micropipette away from the bead. This step was performed at low tension and resulted in tubes with a radius >50 nm. Thereafter, the radius of the tube was decreased in a stepwise manner by increasing membrane tension with micropipette aspiration. At each step and after equilibration, a confocal image was taken along the tube to visualize the fluorescent lipid and the bound protein. In addition, the lateral displacement of the bead relative to the trap centre was followed by video tracking. This permitted to measure the force applied to the tube and to calculate, knowing also the tension value, the tube radius (Sorre *et al*, 2009).

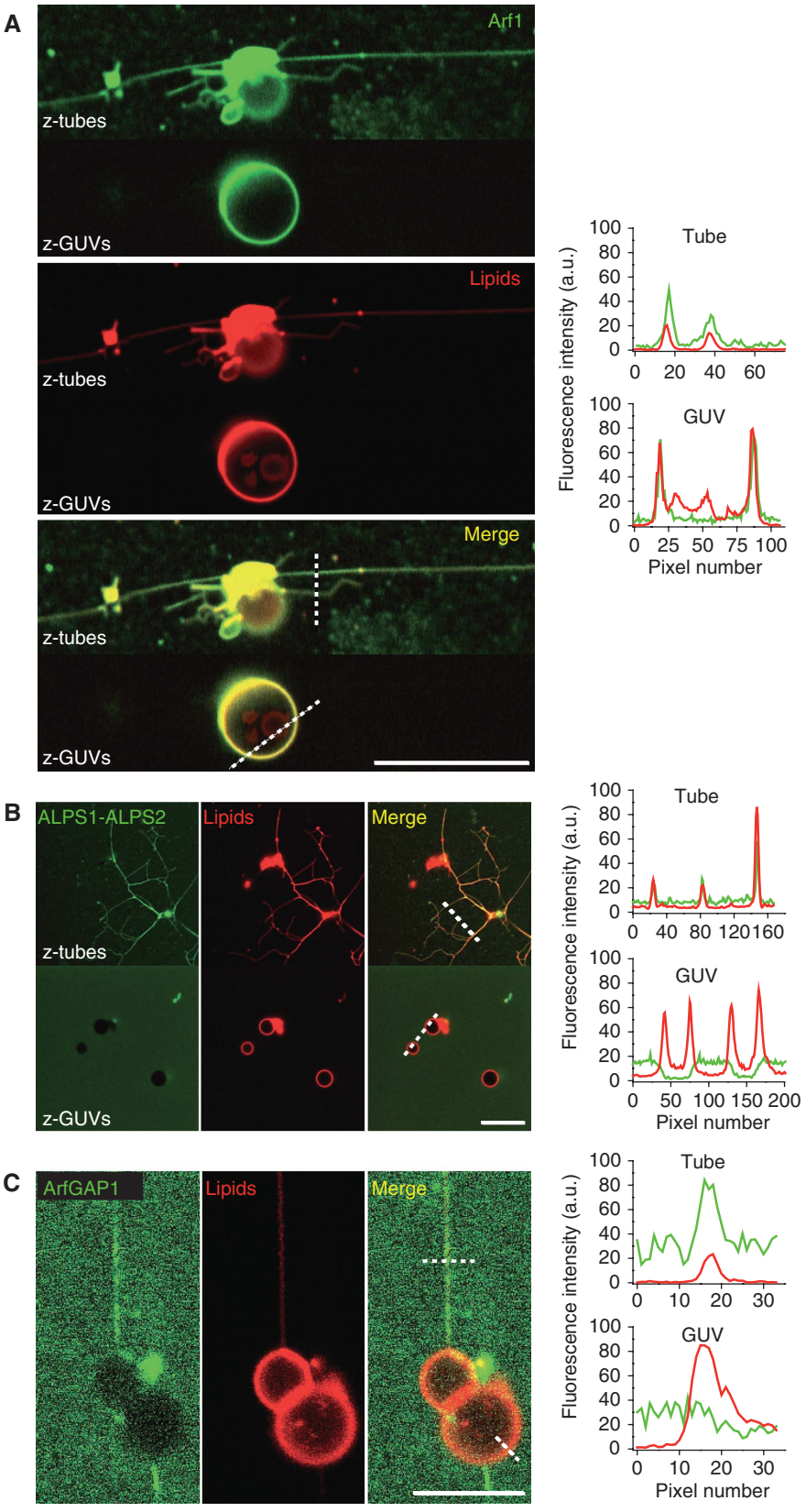

Figure 1 ArfGAP1 and its ALPS1-ALPS2 region bind specifically to curved membranes, whereas Arf1-GTP shows only a slight preference for curved regions. Membrane tube networks were pulled from GUVs containing DOPC (98%), a red fluorescent lipid (BodTRCer, 1%) and a biotinylated lipid (BiotPE, 1%) by the truncated biotinylated version of kinesin 1. Tube networks (red panel) were incubated with 0.5 μM Arf1-OG in the presence of GTP (**A**), 0.5 μM, ALPS1-ALPS2-Alexa^{488} (**B**) or 1 μM ArfGAP1 labelled with a primary antibody against ArfGAP1 (rabbit) and a secondary green fluorescent (Alexa^{488}) anti-rabbit antibody (**C**). Fluorescence intensity profiles in the tube ('z-tubes' in the confocal images on the left panels) and in the GUV ('z-GUVs') regions across the dashed lines are plotted on the right panels (green line: protein fluorescence; red line: lipid marker fluorescence). Scale bar: 15 μm.

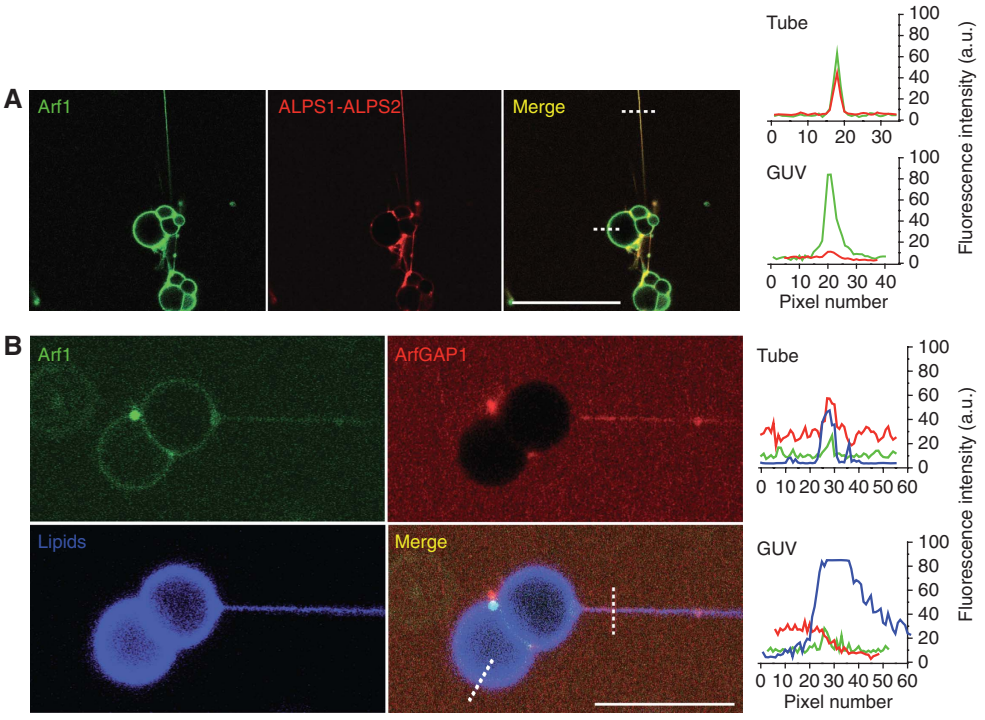

Figure 2 Membrane-bound Arf1-GTP does not alter the ability of ALPS and ArfGAP1 to interact specifically with curved membranes. Kinesin-pulled tube networks were first incubated with 0.5 μM Arf1-OG + GTP (green). Then 3 μM ALPS1-ALPS2-Alexa^{546} (**A**) or 3 μM antibody-labelled ArfGAP1 (**B**) was injected (red). The lipid marker SQUARE-685-PC is shown in (**B**) (blue channel). Fluorescence intensity profiles in the tube and GUV regions across the dashed lines are plotted on the right panels (green line: Arf1-OG fluorescence; red line: ALPS1-ALPS2-Alexa^{546} fluorescence in (**A**) or Cy3 antibody-labelled ArfGAP1 in (**B**); blue line: lipid marker fluorescence). Scale bar: 15 μm.

Supplementary Figure S3A shows a full sequence of images for a GUV incubated with ALPS1-ALPS2-Alexa^{488}. Some selected images and the corresponding quantifications are shown in Figure 3A. During the first steps of aspiration when the tube radius was larger than 36 ± 5 nm (mean ± s.d.; $N = 8$), no binding of ALPS1-ALPS2-Alexa^{488} could be observed. When the radius reached a value of about 35 nm, a green signal was suddenly detected on the tube (Supplementary Figure S3A). This signal then increased gradually as the radius further decreased, whereas the GUV membrane remained unlabelled. To quantify this complex binding behaviour, we plotted the ratio between the ALPS1-ALPS2-Alexa^{488} signal and the fluorescent lipid signal against membrane curvature ($1/R_{tube}$) (Figure 3A, right panel). From these data, a critical radius threshold of 36 ± 5 nm (mean ± s.d.; $N = 8$) for the binding of ALPS1-ALPS2-Alexa^{488} to DOPC tubes was measured. Interestingly, we noticed that the ALPS1-ALPS2-Alexa^{488} peptide also affected the relationship between the force needed to hold the tube and membrane tension (Supplementary Figure S3B and C). On simple membranes, the square of the force depends linearly on membrane tension (Evans and Yeung, 1994). However, a clear downward deviation was observed in the presence of the ALPS1-ALPS2-Alexa^{488} peptide. This suggests that ALPS motifs not only bind specifically to thin membrane tubes, but also induce mechanical effects on the membranes.

Next, we performed similar experiments with Arf1-OG in the presence of GTP. As expected, Arf1-OG was found evenly distributed at the surface of the GUV before the tube was pulled out (Figure 3B). Moreover, as soon as the tube was formed (at low tension when $R_{tube} > 50$ nm), it became immediately labelled with Arf1-OG. Thus, and in contrast to ALPS1-ALPS2-Alexa^{488}, there is no critical radius for Arf1-GTP binding. This further illustrates the quite permissive behaviour of Arf1-GTP as regard to membrane curvature. When the tube radius was stepwise decreased, we observed a clear enrichment of Arf1-OG in the tube region. The ratio between the green (Arf1-OG) and the red (lipid) fluorescence signals across the tube increased by two-fold for tubes displaying a radius close to that of kinesin-pulled tubes (20 nm) and up to six-fold for extremely thin tubes ($R = 8$ nm) (Figure 3B).

Qualitatively, the discontinuous and sharp response of ALPS1-ALPS2- Alexa^{488} to membrane curvature clearly contrasted with the monotonous and weak response of Arf1-OG. However, the curves shown in Figure 3A and B cannot be directly compared because the two proteins do not bear the same fluorescent dye. This problem could be circumvented by calculating a distribution ratio, that is by normalizing the protein/lipid signal ratio in the tube to that observed in the GUV. Although the distribution ratio of ALPS1-ALPS2-Alexa^{488} in the tube was apparently infinite because of the lack of detectable Alexa^{488} signal on the GUV, a lower limit could be determined by considering that the peptide was not excluded from the GUV membrane but bound faintly such as to give a fluorescent signal similar to the background Alexa^{488} signal. We could then directly compare the responses of Arf1-OG and ALPS1-ALPS2-Alexa^{488} to membrane curvature (Figure 3C). Strikingly, and despite the underestimation of its distribution ratio, the response ALPS1-ALPS2-Alexa^{488} to membrane curvature surpassed by a factor of at least 30 the response of GTP-bound Arf1-OG. In addition, ALPS1-ALPS2-

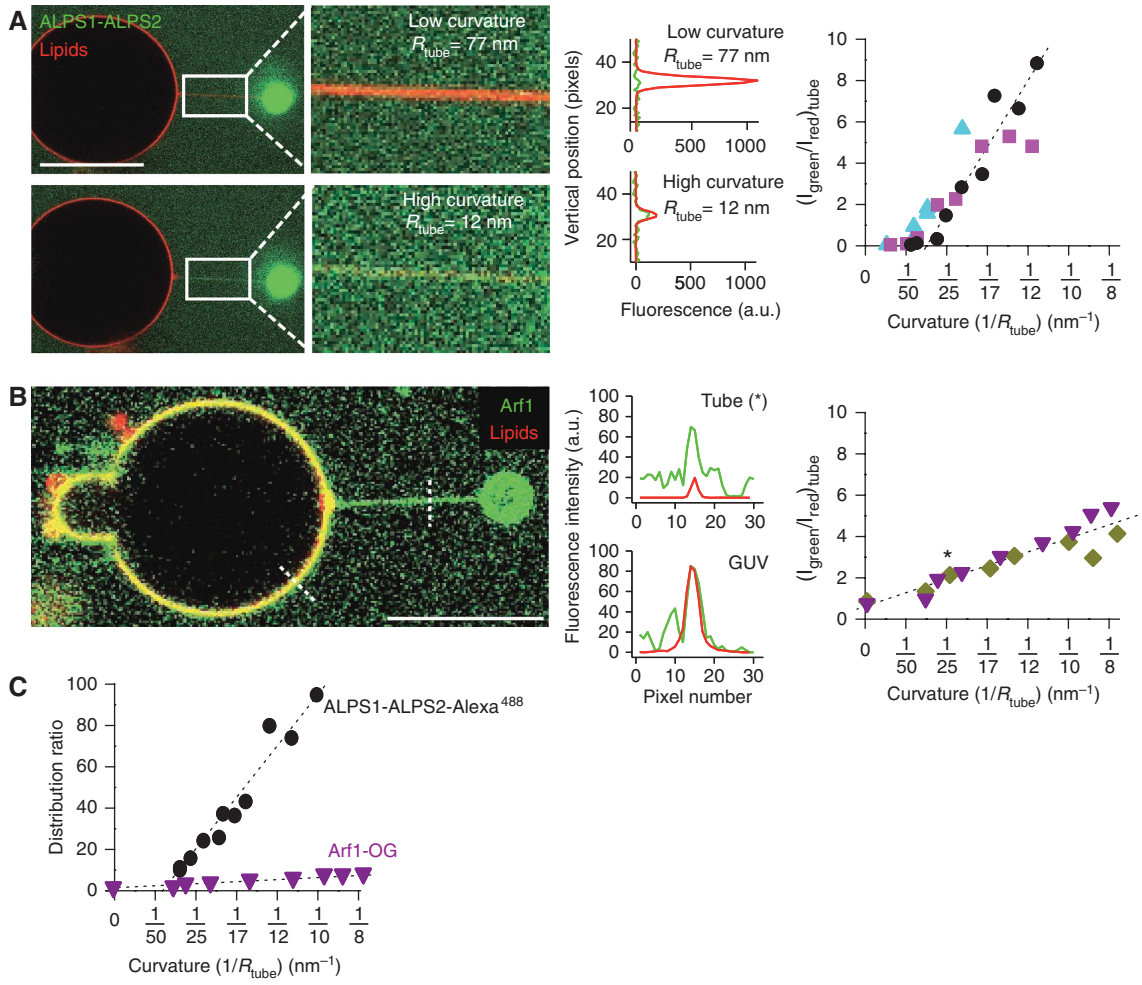

Figure 3 A curvature threshold for the binding of the ALPS1-ALPS2 region of ArfGAP1 to membrane tubes. (**A**) A single membrane tube was pulled with optical tweezers from a DOPC GUV containing the fluorescent lipid marker BodTRCer (red) in the presence of 0.9 μM ALPS1-ALPS2-Alexa^{488} (green). The micropipette used to manipulate the GUV and to control membrane tension is on the left of the image (not shown). The bead appears in green on the right. Zooms of the tube region at low and high curvatures as well as the corresponding fluorescence intensity profiles for ALPS1-ALPS2-Alexa^{488} (green line) and BodTRCer (red line) across the tube are shown. The red signal from the lipid marker is weak at high curvature because of thinning of the tube. The right panel shows the ratio between ALPS1-ALPS2-Alexa^{488} fluorescence (I_{Green}) and the lipid marker fluorescence (I_{Red}) as a function of tube curvature ($1/R_{tube}$) from three representative experiments performed with different GUVs. The intersection between the dotted line and the *x* axis gives the critical curvature radius for ALPS1-ALPS2 binding (36 ± 5 nm). (**B**) Same as in (**A**) except that ALPS1-ALPS2-Alexa^{488} was replaced by 0.5 μM Arf1-OG, which was converted to the GTP-bound conformation in the presence of the GUV before the formation of the tube (two independent experiments). The data point indicated by an asterisk corresponds to fluorescence ratio in the tube shown in the left image. The point at zero curvature corresponds to the fluorescence ratio on the GUV. (**C**) To compare the data shown (**A**, **B**), the fluorescence ratio in the tube was normalized to that in the GUV to get the distribution ratio, which is independent on the experimental conditions (labelling, gain and photobleaching). For this purpose, the ALPS1-ALPS2-Alexa^{488} fluorescence on the GUV was considered to be equal to the background noise. The effect of membrane curvature on the distribution ratio of ALPS1-ALPS2-Alexa^{488} is thus underestimated. Scale bar: 15 μm.

Alexa^{488} was enriched by a factor of 100 or higher in the thinnest tubes ($R = 10$ nm).

Arf1 gradients generated by ArfGAP1 activity on membrane tubes

The above experiments demonstrate that when ArfGAP1 and Arf1-GTP face a membrane displaying flat and curved regions, ArfGAP1 segregates through its ALPS motifs in curved (radius <35 nm) regions, whereas Arf1-GTP distributes more evenly on all regions. An implication of this observation is that GTP hydrolysis on Arf1, which is catalysed by ArfGAP1, should occur exclusively on the curved regions. Moreover, because GTP hydrolysis on Arf1 induces the detachment of the protein from the lipid membrane (see below), local GTP hydrolysis in a tube should lead to loss of the Arf1 signal at this location.

To test this prediction, we first performed experiments in which membrane networks driven by kinesin motors (similar to that used in Figures 1 and 2) were incubated with Arf1-OG and GTP and subsequently exposed to ArfGAP1. The gentle manipulations needed to exchange the solutions in the chamber made this method poorly adapted to kinetic measurements and precluded accurate comparison between different membrane regions. Nevertheless, we observed that ArfGAP1 induced a clear decay of the Arf1-OG signal not only from the tubular regions, as expected, but also from the parental GUV membrane (data not shown). To explain this observation and because the tubular network and the GUVs

are connected, we reasoned that the Arf1 density could decrease on the GUVs because GTP-bound Arf1 diffuses to the tubes. The Arf1 density should then depend not only on the rate of GTP hydrolysis in the tubes, but also on the time needed for GTP-bound Arf1 to diffuse from the GUVs to the tubes.

Experiments performed at low ArfGAP1 concentration and on tubes pulled by optical tweezers turned out to be well adapted to study this potential diffusion–reaction process. In the first stage, DOPC GUVs were incubated with Arf1-OG and with GTP. The GUVs, hence covered with active Arf1-OG, were transferred to a micromanipulation chamber containing 10 nM ArfGAP1 and a membrane tube (radius 10–15 nm) was pulled from a GUV by optical tweezers. At this low ArfGAP1 concentration, the Arf1-OG signal remained stable for several minutes and was analysed by confocal microscopy. Figure 4A shows a typical profile of Arf1-OG on a tube of 17 μm in length. Although some green fluorescence was observed all along the tube, the signal intensity slightly decreased from the base of the tube to its tip. In contrast, the red lipid fluorescence was constant. The non-uniform distribution of Arf1-OG along the tube was suggestive of a diffusion–reaction process: ArfGAP1 activity should be the same along the tubes, but should win at long distance over the lateral diffusion of Arf1-OG from the GUV towards the tube. To better test this, we made very long tubes (about 40 μm) such as to increase the average distance between the location of GTP hydrolysis (the tube) and the reservoir of GTP-bound Arf1 (the GUV). Under these conditions, we could observe a very clear Arf1-OG gradient, with a strong green signal at the base of the tube followed by a regular and complete decrease in the signal up to the tube tip (Figure 4B). In contrast,

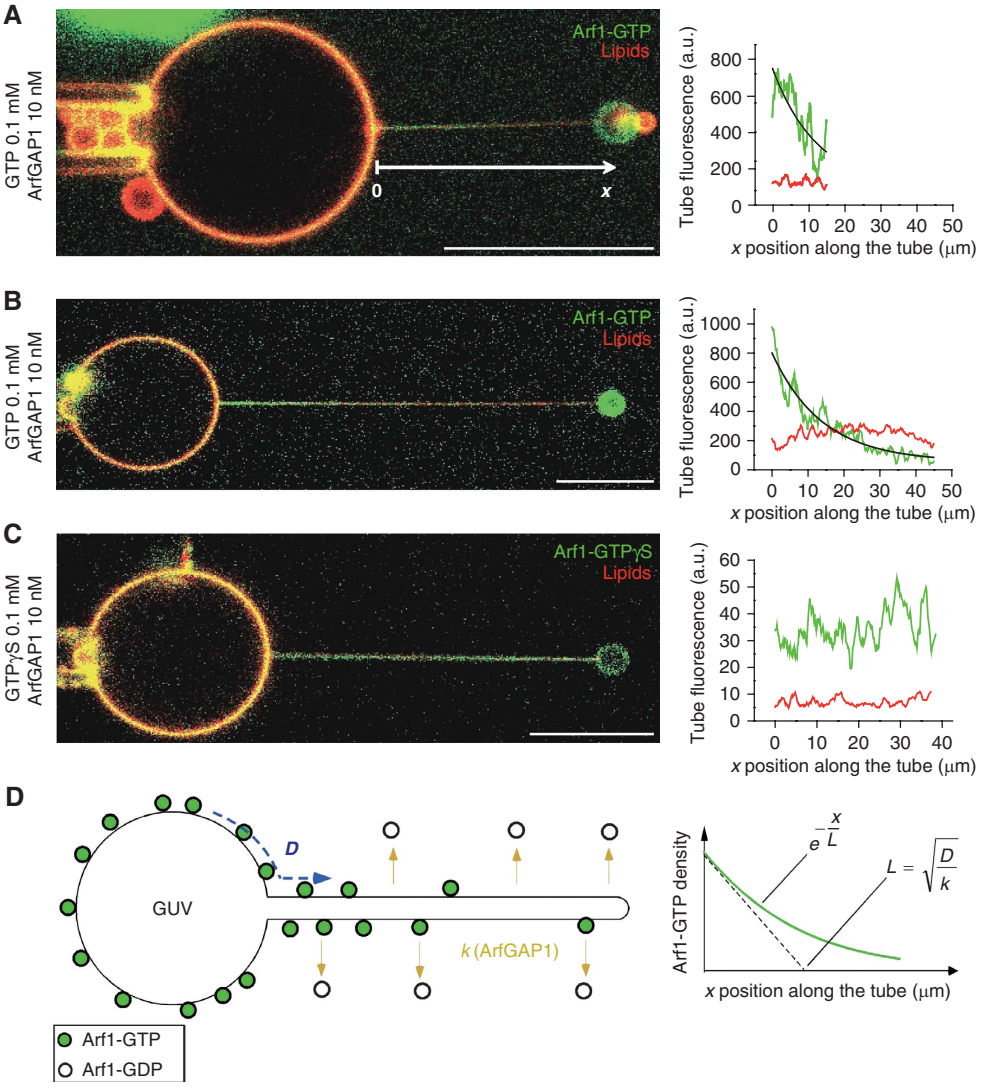

Figure 4 Arf1 gradients induced by ArfGAP1-catalysed GTP hydrolysis on membrane tubes pulled from GUVs. (**A**–**C**) A membrane tube was pulled with optical tweezers from a GUV pre-incubated with Arf1-OG and GTP or the non-hydrolysable analogue GTPγS in the presence of 10 nM ArfGAP1. Tube radius: 10 nm (**A**, **C**) or 15 nm (**B**). The fluorescence intensities of Arf1-OG (green) and the lipid marker (red) along the tube are plotted on the right panels. In (**A**, **B**), Arf1-OG fluorescence intensity was fitted by an exponential decay (black curve). (**D**) Schematic view of the diffusion–reaction model. GTP hydrolysis on Arf1 occurs exclusively on the tube because of specific binding of ArfGAP1 to this region. New Arf1-GTP molecules diffusing from the GUV replace those that dissociate from the tube on GTP hydrolysis. As a result, an Arf1-GTP gradient forms. The characteristic length (L) of the gradient reflects the balance between diffusion (D) and GTP hydrolysis (k). Scale bar: 15 μm.

Arf1-OG, which had been activated by GTPγS, a non-hydrolysable analogue of GTP, was found evenly distributed along the tube (Figure 4C). Taken together, these experiments demonstrate that on a membrane displaying flat and curved regions there is a competition between Arf1-GTP diffusion and localized GTP hydrolysis catalysed by Arf1-GAP1.

To analyse the Arf1 gradients generated by ArfGAP1 in a quantitative manner, we considered a simple diffusion–reaction model (Figure 4D). In the GTP-bound conformation, Arf1 diffuses from the GUV into the tube with a diffusion coefficient D and dissociates from the tube on ArfGAP1-catalysed GTP hydrolysis with a rate constant k. Under steady-state conditions, the model predicts that the concentration of Arf1 should decrease exponentially along the main tube axis with a characteristic length, L (see equation 1 in Materials and methods). Fitting the experimental data (black line in Figure 4B, right panel) gave $L = 8.4 \pm 0.5\,\mu m$ (s.e.m; $N = 9$). The characteristic length is the square root of D/k ($L = \sqrt{D/k}$) and therefore is a direct index of the competition between diffusion and GTP hydrolysis. A shallow gradient (large value of L) is indicative of fast diffusion and/or a slow GTP hydrolysis, whereas a sharp gradient (small value of L) is indicative of slow diffusion and/or fast GTP hydrolysis.

We next wondered whether the value of L given by the membrane pulling experiment was compatible with the values of D and k that could be inferred from other experimental approaches. Using fluorescence recovery after photobleaching (FRAP) experiments, we reported earlier a value of $D = 4.7\,\mu m^2\,s^{-1}$ for the diffusion coefficient of GTP-bound Arf1-OG on giant vesicles displaying a Golgi-like composition (Manneville *et al*, 2008). As shown in Figure 5A, a similar diffusion coefficient was observed for the diffusion of Arf1-OG on DOPC giant vesicles ($D = 3.5\,\mu m^2\,s^{-1}$). Arf-OG also diffuses rapidly on thin DOPC tubes pulled by optical tweezers, although the time resolution of the experiment did not permit us to determine the exact diffusion coefficient (D in the order of $10\,\mu m^2\,s^{-1}$; Figure 5B). To estimate the rate constant of Arf1-OG detachment on GTP hydrolysis, we performed bulk measurements using small DOPC liposomes obtained by extrusion through polycarbonate filters (pore size 0.03 μm). These liposomes had a radius of 40 ± 10 nm as estimated by dynamic light scattering. As the total curvature of a spherical liposome is similar to that of a tube with a two-fold smaller radius, our kinetics measurements should be relevant for tubes displaying radii in the range of 20 nm. As schematized in Figure 5C, we followed the conformational changes of Arf1-OG on GDP to GTP exchange and GTP hydrolysis using tryptophan fluorescence (Antonny *et al*, 1997) and its membrane association–dissociation cycle using fluorescence resonance energy transfer between OG and the fluorescent lipid Rhodamine-PE (Manneville *et al*, 2008). In the first stage, GDP to GTP exchange was promoted by the addition of GTP and by lowering the concentration of magnesium using EDTA. Translocation of Arf1-OG to the liposome surface results in an increase in the fluorescence of Rhodamine (the acceptor) at the expense of the fluorescence of OG (the donor), which was followed here (Figure 5C; green trace). Thereafter, GTP hydrolysis was initiated by the addition of ArfGAP1. The OG fluorescence (green trace) and the tryptophan fluorescence (blue trace) varied in a coordinated manner, suggesting that the membrane association–dissociation cycle of Arf1-OG was in phase with its GDP/GTP cycle (Figure 5C). Notably, Arf1-OG dissociated from the liposomes on ArfGAP1 addition with the same kinetics as Arf1-OG conformational change on GTP hydrolysis. The rate also increased with ArfGAP1 concentration (Figure 5C, inset). In the presence of 10 nM ArfGAP1, k was estimated to be $\approx 2.2 \times 10^{-2}\,s^{-1}$. Using this value and the value of D given by the FRAP experiments we find $L = \sqrt{D/k} = 13\,\mu m$. The calculated characteristic length of the Arf1-OG gradient along the tube is thus in good agreement with the observed value (8.4 μm).

Discussion

The recruitment of proteins involved in the formation of transport vesicles seems remarkably well orchestrated *in vivo* (Kaksonen *et al*, 2005). This may be due in part to the ability of some proteins to finely recognize the morphological changes of the membrane, which occur during budding. Using membrane networks consisting of thin ($R =$ 10–100 nm) tubes emerging from GUVs ($R > 5\,\mu m$), we have investigated the behaviour of Arf1-GTP and ArfGAP1, two proteins that control the assembly–disassembly cycle of the COPI coat, on membranes displaying a topology relevant for intermediate stages of vesicle formation.

ArfGAP1 is hypersensitive to membrane curvature whereas Arf1 binds to flat membranes

The differential distribution of ArfGAP1 and Arf1-GTP on GUV/tube networks is clear cut. ArfGAP1 binds exclusively to the tubes whereas Arf1-GTP shows a permissive behaviour with regard to membrane curvature, distributing both on the tubes and on the GUVs (Figures 1–3). Strikingly, the binding of ArfGAP1 to DOPC tubes occurs below a threshold radius of $R = 36 \pm 5$ nm (Figure 3A and Supplementary Figure S3). Therefore, in the duo formed by ArfGAP1 and Arf1-GTP, the exquisite sensor of membrane curvature is ArfGAP1 and not Arf1-GTP. This conclusion is at odds with the recent claim that proteins of the Arf family sense membrane curvature (Lundmark *et al*, 2008). Such an assertion is based on the fact that liposome size has a weak effect on the rate of Arf1 and Arf6 activation at low magnesium concentration. Typically, reducing liposome radius from 150 to 30 nm increases the rate and extent of spontaneous GDP to GTP exchange on Arf by a factor of ≈1.3. On the other hand, the same decrease in liposome size causes a 30- to 100-fold increase in the rate of ArfGAP1-catalysed GTP hydrolysis on Arf1 (compare Figure 2a in Lundmark *et al*, 2008 and Figure 1c in Bigay *et al*, 2003). Therefore, we argue that the weak sensitivity of Arf1 to membrane curvature, which is also observed here (Figures 1A and 3B), is marginal compared to that of ArfGAP1 on the same lipid membrane system, either GUV/tube networks (this study) or extruded liposomes of defined size (Bigay *et al*, 2003, 2005; Mesmin *et al*, 2007; Drin *et al*, 2008).

If not required for the activation of Arf1, membrane curvature can result from the accumulation of Arf1-GTP on lipid membranes. Under our experimental conditions (submicromolar protein concentration), Arf1-GTP does not deform the GUV surface unless coatomer is subsequently added (Manneville *et al*, 2008). Others have reported that Arf1-GTP in the absence of coatomer but at higher concentration (typically 10 μM) promotes the formation of tubes from liposomes or from lipid membrane sheets (Beck *et al*, 2008;

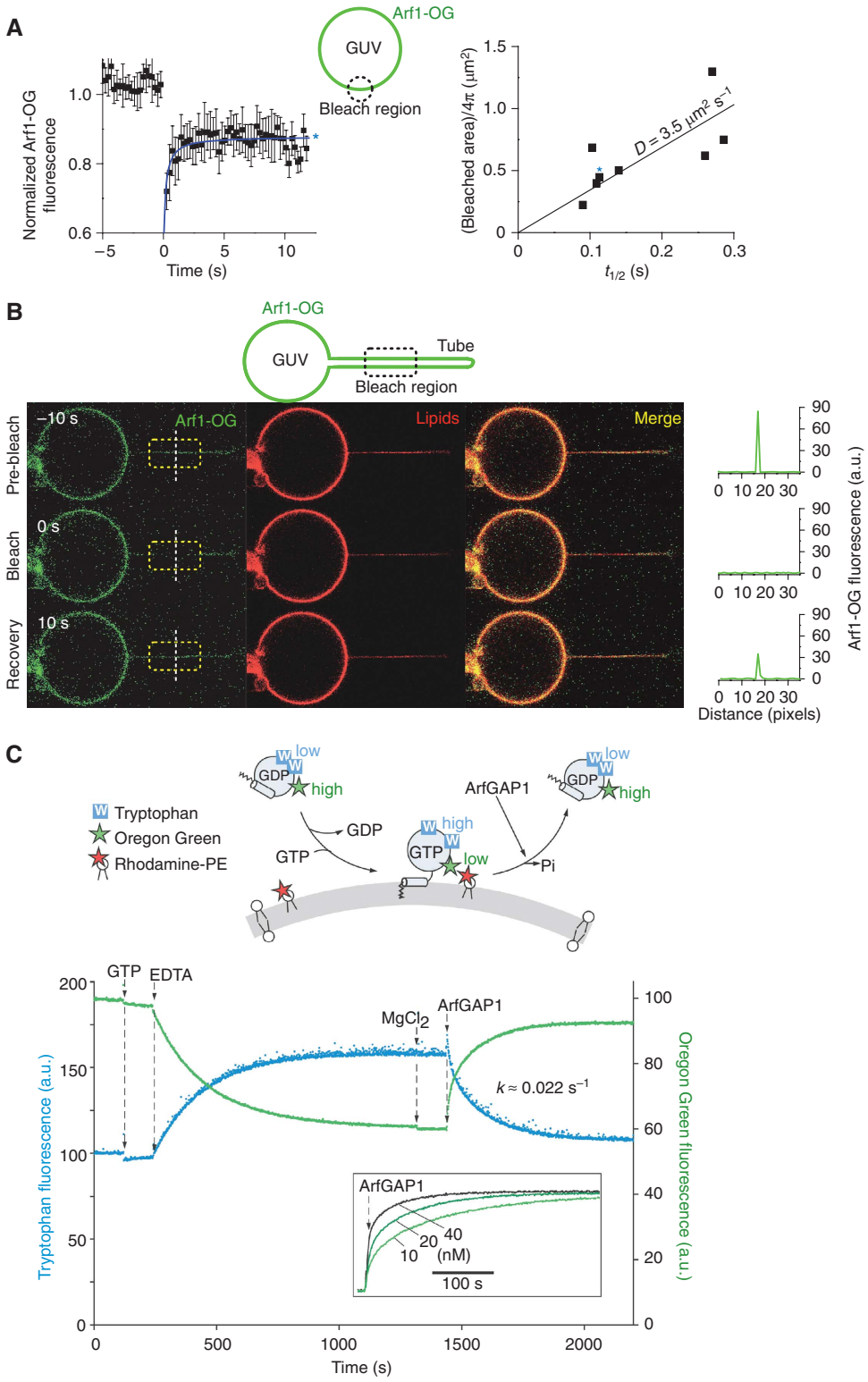

Figure 5 Diffusion coefficient of Arf1-OG and rate constant of ArfGAP1-catalysed GTP hydrolysis on model DOPC membranes. (**A**) Left: typical FRAP curve for GTP-bound Arf1-OG on a DOPC giant vesicle. Right: correlation between the half time of recovery ($t_{1/2}$) and the bleached area (πR^2). The diffusion coefficient is given by $D = R^2/(4t_{1/2})$. (**B**) FRAP experiment showing the fast mobility of GTP-bound Arf1-OG on a DOPC tube pulled by optical tweezers. The length of the photobleached area is 12 μm. (**C**) Top: cartoon representation of the fluorescence signals used to follow either the conformational changes of Arf1-OG on nucleotide exchange and GTP hydrolysis or its binding to and dissociation from small DOPC liposomes. Bottom: Arf1-OG (0.5 μM) was mixed with DOPC small liposomes (0.4 mM; hydrodynamic radius = 40 ± 10 nm) containing 1 mol% Rhodamine-PE. At the indicated times, GTP (40 μM), EDTA (2 mM), $MgCl_2$ (2 mM) and ArfGAP1 (10 nM) were added. Tryptophan fluorescence (blue trace) or Oregon Green fluorescence (green trace) was followed in real time. Note the good time correlation between the two recordings. The inset shows the time course of Arf1-OG dissociation as monitored by Oregon Green fluorescence using increasing concentrations of ArfGAP1.

Krauss *et al*, 2008; Lundmark *et al*, 2008). These observations are not necessarily contradictory. Membrane deformation on COPI-coat assembly probably arises from two factors that act in a synergistic manner: the 'wedge' effect of Arf1-GTP, which should be significant at high surface density when several Arf1-GTP molecules are trapped in a small coated area, and the coat itself, owing to its spherical scaffold structure. However, Arf and Arf-like proteins recruit not only coat proteins but also various effectors such as golgins and lipid-modifying enzymes (Gillingham and Munro, 2007). These interactions do not seem to require or induce membrane curvature: for instance, the complex between Arf1-GTP and the C-terminal region of the golgin GMAP-210 forms readily on flat membranes (Drin *et al*, 2008). It should be also noted that in early electron microscopy studies on Golgi membrane preparations, Arf1 was detected on flat cisternae whereas efficient membrane deformation was observed only after the addition of coatomer (Orci *et al*, 1993a, b). In conclusion, if membrane curvature is inherent of some mechanisms that are controlled by Arf1, this small G protein interacts quite well with flat membranes and the mechanisms by which membrane curvature is either induced or sensed depend largely on the recruitment of other proteins such as coat complexes or ArfGAP1, respectively.

A diffusion–reaction model for the stabilization of the COPI coat

The sharp dependency of ArfGAP1 on membrane curvature has key implications for the distribution of the GTPase reaction during COPI budding. The fact that there is a threshold radius of 35 nm for the binding of the ALPS1-ALPS2 motif of ArfGAP1 (Figure 3A) suggests that 'early' buds displaying a shallow curvature should be protected from ArfGAP1 (Figure 6A). However, this should not be the case for 'late' buds displaying a curvature close to the final vesicle. We suggested earlier that the dissociation of Arf1 molecules could be tolerated if the coat lattice is sufficiently stabilized by lateral contacts (Figure 6A; Bigay *et al*, 2003). The experiments presented here suggest that diffusion of Arf1-GTP from the parental flat membrane into the bud is an additional factor that could contribute to the stability of coated buds (Figure 6B).

When a catalytic amount of ArfGAP1 was added to GUV/tube networks covered with Arf1-GTP, preferential loss of Arf1 from the tubes was evident only for very long tubes, which showed an exponential decrease in Arf1 density from the base of the tube to its tip with a characteristic length in the range of $\approx 10\,\mu m$ (Figure 4B). This suggests that dissociation of Arf1 in highly curved regions can be readily compensated over short distance (sub-micrometer) by lateral diffusion.

About 100 nm separate the tip of a COPI bud from the parental Golgi cisternae (Figure 6A and B). To generate a sharp Arf1 gradient over this distance range, our model predicts that extremely high values of k and extremely low values of D are needed. In Figure 6C, we plotted pair values of D and k that give a characteristic length $L = 50\,nm$. If Arf1 diffuses freely in the bud ($D \approx 3$–$5\,\mu m^2\,s^{-1}$; Figure 5A; Manneville *et al*, 2008), k should be in the order of $2000\,s^{-1}$. This largely exceeds the fastest reported rates of GTP hydrolysis in G protein–GAP complexes (in the range of $10\,s^{-1}$; Ahmadian *et al*, 1997). Conversely, if GTP hydrolysis

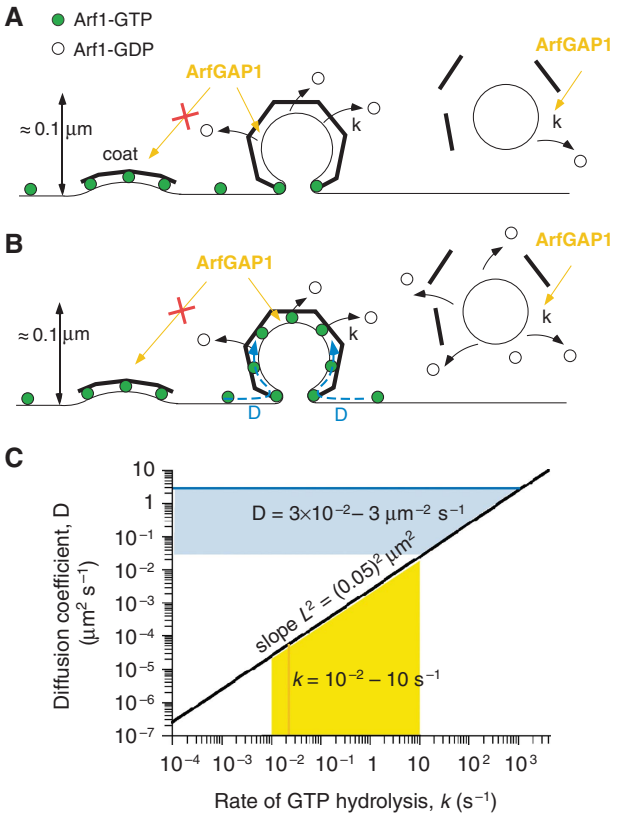

Figure 6 Implications of the diffusion–reaction model for the stability of the COPI coat during budding. (**A**) With no lateral diffusion of Arf1 a mature COPI-coated bud should have lost most of its Arf1-GTP molecules through the action of ArfGAP1, which acts in regions of high positive curvature. This could compromise coat stability. (**B**) Alternatively, new Arf1-GTP molecules diffusing from the Golgi cisternae could constantly replace those that are leaving the bud on GTP hydrolysis, thereby stabilizing the coat. Once membrane fission occurs, the flux of Arf1-GTP necessarily stops and GTP hydrolysis on Arf1 leads to coat disassembly from the vesicle. (**C**) The black line of the plot reports pair values of k and D that leads to an Arf1 gradient with a characteristic length $L = 50\,nm$. The bold coloured lines indicate the values of k and D given by the experiments shown in Figure 5. The yellow area shows the range of reported values for the rate constant (k) of GTP hydrolysis on Arf1 catalysed by ArfGAP1. The blue area describes the range of D-values that would prevent the formation a sharp Arf1-GTP gradient in a curved region of the size of a COPI-coated bud when this region is connected to a flat membrane serving as a reservoir of Arf1-GTP.

in the COPI bud occurs with a time constant $k = 10\,s^{-1}$, D should be in the order of $2.5 \times 10^{-2}\,\mu m^2\,s^{-1}$, that is 0.5–1% the diffusion of Arf1 on a pure lipid membrane (Figure 5A; Manneville *et al*, 2008). We conclude that a significant decrease in the density of Arf1-GTP in a COPI bud requires not only a very fast rate of GTP hydrolysis in this area but also a very slow rate of protein lateral diffusion.

Live cell imaging approaches with fluorescent proteins have begun to give information on the dynamics of proteins of the COPI machinery *in vivo* (Vasudevan *et al*, 1998; Presley *et al*, 2002; Liu *et al*, 2005). Notably, they permit to estimate the overall time needed for Arf1, ArfGAP1 and coatomer to cycle between the cytosol and the Golgi and clearly indicate an intimate link between these association–dissociation events. Despite these progresses, however, we are far from knowing the duration of individual steps, such as the time

needed for Arf1-GTP to diffuse at the surface of a single Golgi cisternae or the lifetime of Arf1-GTP in a COPI bud. Complications arise from the small size and the complex structure of the Golgi, from the fact that Arf1-GTP recruits various effectors on this organelle and from the involvement of at least two ArfGAPs. In the case of COPI-coated buds, the rate of GTP hydrolysis catalysed by ArfGAP1 is probably controlled not only by membrane curvature, but also by interactions between ArfGAP1, the COPI coat and cargo molecules (Szafer *et al*, 2001; Liu *et al*, 2005; Levi *et al*, 2008). Moreover, it is not clear whether ArfGAP1 acts in a catalytic or in a stoechiometric manner (Yang *et al*, 2002). In our experiments, ArfGAP1 was used in catalytic amount compared to Arf1 (1:40 ratio). If we extrapolate the observed value of k for a stoechiometric amount of ArfGAP1, the rate constant of GTP hydrolysis would be in the range of $1\,s^{-1}$. This large uncertainty in the value of k is illustrated by the yellow area in Figure 6C, which depicts values from 10^{-2} to $10\,s^{-1}$.

The lateral mobility of Arf1-GTP on Golgi cisternae is not precisely known because values of D given by FRAP experiments probably integrate several steps including the cycling of Arf between the cytosol and membranes (Vasudevan *et al*, 1998; Presley *et al*, 2002). Peripheral proteins that are anchored in cellular membranes through lipid modifications display D values in the range of $0.3–1\,\mu m^2\,s^{-1}$ (Kenworthy *et al*, 2004). If this range seems reasonable for the lateral mobility of Arf1-GTP before its engagement in the coat, it is likely that the COPI lattice and the high density of proteins at the neck region should make the exchange of Arf1 molecules between the parental membrane and the bud much less efficient. However, this is difficult to address experimentally. Notwithstanding this, our data suggest that, unless diffusion of Arf1-GTP in the COPI-coat lattice is completely impaired, even a modest flux ($>1\%$ of unrestricted diffusion, i.e. $3\times10^{-2}\,\mu m^2\,s^{-1}$) of Arf1-GTP molecules coming from the parental membrane could overcome the loss of Arf1 by GTP hydrolysis in the bud. This is illustrated by the blue area in Figure 6C, which describes the range of D-values that would counteract GTP hydrolysis when k varies up to $10\,s^{-1}$. Interestingly, FRAP experiments in living cells suggest that the assembly–disassembly cycle of the COPI coat is not in phase with the GTPase cycle of Arf1. Arf1 cycles more rapidly between the cytosol and the Golgi membrane than coatomer, although coatomer depends on GTP hydrolysis on Arf1 for its cycling (Presley *et al*, 2002; Liu *et al*, 2005). Therefore, we propose that coat expansion and polymerization during budding is accompanied by cycling of Arf1 molecules, which enter the bud by lateral diffusion and leaves it by GTP hydrolysis, thus permitting the coat to remain metastable (Figure 6B).

One of the most interesting aspects of this model is that it makes membrane fission the triggering event for coat disassembly. When the neck is cut, the loss of Arf1 by GTP hydrolysis is no longer compensated by Arf1-GTP diffusion (Figure 6B). As a result, the coat should readily disassemble. Importantly, such a mechanism is valid not only for GAPs that are regulated by membrane curvature but also for those that are regulated by coat assembly (Futai *et al*, 2004; Sato and Nakano, 2005; Weimer *et al*, 2008; Kliouchnikov *et al*, 2009; Schindler *et al*, 2009). The only prerequisite for these diffusion-based models is that exchange factors must be excluded from coated vesicles.

Materials and methods

A detailed description of the various reagents and of the protocols used for protein expression, purification and labelling is provided as Supplementary data.

Giant unilamellar vesicles

GUVs containing 99 mol% DOPC and 1 mol% Bodipy-TR-Ceramide or SQUARE-685-PC were grown on ITO slides or platinum wires using the electro formation technique (Angelova *et al*, 1992). GUV formation was performed at room temperature in sucrose solutions matching the osmolarity of the buffers used for the various experiments. To allow adhesion between the membrane and the streptavidin–biotinylated kinesin (tube pulling by kinesin), the biotinylated lipid Biot-Cap-DOPE was added at 1% mole. To achieve the same adhesion with streptavidin-coated beads, 0.03% mole of DSPE-PEG(2000)-Biotin was used (tube pulling by optical tweezers).

Membrane tube pulling by biotinylated kinesin

The assay was performed as published before (Leduc *et al*, 2004). Briefly, polymerized microtubules in BRB80 buffer (80 mM Pipes pH 6.8, 1 mM $MgCl_2$, 1 mM EGTA) were adsorbed to the coverslip of a micro-flow chamber ($\sim5\,\mu l$) for 10–20 min. The chamber was then incubated with casein $5\,mg\,ml^{-1}$ in HKM buffer (50 mM Hepes pH 7.2, 120 mM KAcetate, 1 mM $MgCl_2$) supplemented with 2 mM EGTA for 10 min. Excess casein was rinsed with HKM containing 5 mM DTT and 33 μM taxol (HKM-DTT-TX). A solution of biotinylated kinesin, incubated earlier with streptavidin ($\sim0.16\,mg\,ml^{-1}$ in HKM-DTT-TX), was then injected into the chamber for 20 min. Thereafter, the microtubule/kinesin-containing chamber was rinsed with motility buffer (MB: HKM-DTT-TX + 1.5 mM ATP). GUVs matching the osmolarity of MB were injected onto the top of the chamber and incubated for 10 min at room temperature. Confocal images were taken either on a Zeiss LSM-META or a Nikon CS1 microscope using a $\times63$ or a $\times60$ objective, respectively. Green-emitting dyes were excited with a 488 nm laser. Red-emitting dyes were excited at 543 nm (Zeiss) or 561 nm (Nikon).

Membrane tube pulling at controlled membrane tension by optical tweezers

The setup was recently described in Sorre *et al* (2009). For each experiment, a 100–200 μl open micromanipulation chamber was built with two clean glass coverslips. To prevent adhesion of the GUVs to the glass, the surfaces of the chamber and of the micropipette were incubated with $10\,mg\,ml^{-1}$ β-casein (10 min) and then rinsed with HKM. To monitor ALPS binding, 100–200 μl of 1 μM ALPS1-ALPS2-Alexa^{488} in HKM was injected into the chamber and 3.2 μm-diameter streptavidinated-polystyrene beads were supplemented. GUVs of 5 μl were then transferred from the growth chamber to the micromanipulation chamber. The sample was sealed with mineral oil to prevent water evaporation.

For ArfGAP1 activity experiments, DOPC GUVs of 5 μl were added, in an eppendorf tube, to a 75 μl solution containing 2 μM Arf1-OG, 2 mM EDTA and 0.1 mM GTP in HKM buffer, followed by incubation for 20 min at RT. To remove excess Arf1-OG, the GUVs were centrifuged at 600 r.p.m. for 10 min; 70 μl of the supernatant was discarded and 90 μl of HKM, EDTA 2 mM, GTP 0.1 mM was added at each step. Washing was repeated three times. The liposome suspension was then supplemented with ArfGAP1 (final concentration 10 nM) or ArfGAP1 buffer (control) and incorporated into the working chamber.

Membrane tension of the GUV varied from 5×10^{-6} to $2\times10^{-4}\,N\,m^{-1}$ by micropipette aspiration (Evans and Rawicz, 1990) allowing the formation of tubes with radii from 10 to 200 nm. Membrane tubes with a large radius were pulled from giant vesicles with a low initial membrane tension (i.e. displaying optically visible membrane fluctuations). The tube was formed from the giant vesicle after adhesion of an optically trapped streptavidin-coated bead and extended to a length of 10–50 μm by moving the pipette away from the bead. The tube length was kept constant during the whole experiment. Membrane tension was then increased in a stepwise manner. For each tension, the position of the bead relative to the centre of the trap was recorded by video microscopy (force quantification) and the fluorescence signal of the lipid dye in the membrane was quantified using confocal microscopy. At least 1 min was left after each data point to allow membrane composition to equilibrate within the tube by diffusion.

Before each experiment, zero aspiration pressure in the pipette was calibrated by looking at the movement of a bead inside the pipette. All experiments were performed at room temperature (21 ± 1°C).

Fluorescence quantification

To quantify peptide binding, the fluorescence intensity of ALPS1-ALPS2-Alexa^{488} (I_{green}) was normalized to the intensity of the fluorescent lipid (BodTRCer, I_{red}) after each increasing tension step (see Figure 3; Supplementary Figure S3). I_{green} and I_{red} were measured from a rectangular region of interest that included the horizontal tube. These 2D data sets were transformed into a 1D array by averaging along vertical lines, leading to a strong increase in the signal-to-noise ratio. The fluorescence ratio I_{green}/I_{red} in the tube was calculated after subtracting the noise level to the maximum of the fluorescence peak for each dye. Arf1-OG fluorescence along the tube in the presence or in the absence of ArfGAP1 was quantified in the same way.

Diffusion–reaction model

We considered a simple diffusion–reaction model in which Arf1 diffuses from the GUV to the tube with a diffusion coefficient D and is removed from the tube through ArfGAP1-catalysed GTP hydrolysis at a rate constant k. The tube is described as a 1D system along the x axis. At steady state, the diffusion–reaction equation describing the concentration profile of Arf1-OG along the tube $c(x)$ is:

$$\partial c/\partial t = D\partial^2 c/\partial x^2 - kc = 0$$

This gives:

$$c(x) = c_0 e^{-x/L} + cst \quad (1)$$

where c_0 is the Arf1-OG fluorescence signal at the base of the tube, x is the position along the tube, cst a constant and $L = \sqrt{D/k}$ is the characteristic length of the Arf1 gradient along the tube.

Fluorescence measurements of the GTPase and membrane translocation cycles of Arf1-OG

Measurements were performed in a quartz cuvette containing 0.5 μM Arf1-OG (initially in the GDP-bound form) and 0.4 mM DOPC liposomes (radius 40 ± 10 nm and containing 1 mol% Rhodamine-PE) in HKM buffer. The suspension was stirred with a small magnetic bar. Reagents were sequentially added from stock solutions using Hamilton syringes. Arf1-OG tryptophan fluorescence was measured at 340 nm on excitation at 297.5 nm. OG fluorescence was measured at 520 nm on excitation at 490 nm.

Supplementary data

Supplementary data are available at *The EMBO Journal* Online (http://www.embojournal.org).

Acknowledgements

This work was supported by the Centre National de la Recherche Scientifique (CNRS), the Institut Curie, and a grant from the Agence Nationale de la Recherche (ANR-05-BLAN-0095). BS was supported by grants from the Direction Générale pour l'Armement, from the CNRS and from the Fondation pour la Recherche Médicale. We thank Dan Cassel for ArfGAP1 antibody and all members of our labs for discussion and help. We thank the PICT-IBISA imaging platform and the NIKON imaging center @ Institut Curie for assistance in confocal microscopy.

Conflict of interest

The authors declare that they have no conflict of interest.

References

Ahmadian MR, Hoffmann U, Goody RS, Wittinghofer A (1997) Individual rate constants for the interaction of Ras proteins with GTPase-activating proteins determined by fluorescence spectroscopy. *Biochemistry* **36:** 4535–4541

Angelova M, Soléau S, Méléard P, Faucon F, Bothorel P (1992) Preparation of giant vesicles by external AC electric fields. Kinetics and applications. In *Trends in Colloid and Interface Science VI,* C Helm, M Lösche, H Möhwald (eds), pp 127–131. Steinkopff Verlag-Darmstadt, Springer-Verlag-New York: Springer Berlin/Heidelberg

Antonny B, Beraud-Dufour S, Chardin P, Chabre M (1997) N-terminal hydrophobic residues of the G-protein ADP-ribosylation factor-1 insert into membrane phospholipids upon GDP to GTP exchange. *Biochemistry* **36:** 4675–4684

Beck R, Sun Z, Adolf F, Rutz C, Bassler J, Wild K, Sinning I, Hurt E, Brugger B, Bethune J *et al.* (2008) Membrane curvature induced by Arf1-GTP is essential for vesicle formation. *Proc Natl Acad Sci USA* **105:** 11731–11736

Bigay J, Gounon P, Robineau S, Antonny B (2003) Lipid packing sensed by ArfGAP1 couples COPI coat disassembly to membrane bilayer curvature. *Nature* **426:** 563–566

Bigay J, Casella JF, Drin G, Mesmin B, Antonny B (2005) ArfGAP1 responds to membrane curvature through the folding of a lipid packing sensor motif. *EMBO J* **24:** 2244–2253

Drin G, Morello V, Casella JF, Gounon P, Antonny B (2008) Asymmetric tethering of flat and curved lipid membranes by a golgin. *Science* **320:** 670–673

Evans E, Rawicz W (1990) Entropy-driven tension and bending elasticity in condensed-fluid membranes. *Phys Rev Lett* **64:** 2094–2097

Evans E, Yeung A (1994) Hidden dynamics in rapid changes of bilayer shape. *Chem Phys Lipids* **73:** 39–56

Frigerio G, Grimsey N, Dale M, Majoul I, Duden R (2007) Two human ARFGAPs associated with COP-I-coated vesicles. *Traffic* **8:** 1644–1655

Futai E, Hamamoto S, Orci L, Schekman R (2004) GTP/GDP exchange by Sec12p enables COPII vesicle bud formation on synthetic liposomes. *EMBO J* **23:** 4146–4155

Gillingham AK, Munro S (2007) The small G proteins of the Arf family and their regulators. *Annu Rev Cell Dev Biol* **23:** 579–611

Kaksonen M, Toret CP, Drubin DG (2005) A modular design for the clathrin- and actin-mediated endocytosis machinery. *Cell* **123:** 305–320

Kenworthy AK, Nichols BJ, Remmert CL, Hendrix GM, Kumar M, Zimmerberg J, Lippincott-Schwartz J (2004) Dynamics of putative raft-associated proteins at the cell surface. *J Cell Biol* **165:** 735–746

Kliouchnikov L, Bigay J, Mesmin B, Parnis A, Rawet M, Goldfeder N, Antonny B, Cassel D (2009) Discrete determinants in ArfGAP2/3 conferring Golgi localization and regulation by the COPI coat. *Mol Biol Cell* **20:** 859–869

Krauss M, Jia JY, Roux A, Beck R, Wieland FT, De Camilli P, Haucke V (2008) Arf1-GTP-induced tubule formation suggests a function of Arf family proteins in curvature acquisition at sites of vesicle budding. *J Biol Chem* **283:** 27717–27723

Leduc C, Campas O, Zeldovich KB, Roux A, Jolimaitre P, Bourel-Bonnet L, Goud B, Joanny JF, Bassereau P, Prost J (2004) Cooperative extraction of membrane nanotubes by molecular motors. *Proc Natl Acad Sci USA* **101:** 17096–17101

Levi S, Rawet M, Kliouchnikov L, Parnis A, Cassel D (2008) Topology of amphipathic motifs mediating Golgi localization in ArfGAP1 and its splice isoforms. *J Biol Chem* **283:** 8564–8572

Liu W, Duden R, Phair RD, Lippincott-Schwartz J (2005) ArfGAP1 dynamics and its role in COPI coat assembly on Golgi membranes of living cells. *J Cell Biol* **168:** 1053–1063

Lundmark R, Doherty GJ, Vallis Y, Peter BJ, McMahon HT (2008) Arf family GTP loading is activated by, and generates, positive membrane curvature. *Biochem J* **414:** 189–194

Manneville JB, Casella JF, Ambroggio E, Gounon P, Bertherat J, Bassereau P, Cartaud J, Antonny B, Goud B (2008) COPI coat assembly occurs on liquid-disordered domains and the associated membrane deformations are limited by membrane tension. *Proc Natl Acad Sci USA* **105:** 16946–16951

Mesmin B, Drin G, Levi S, Rawet M, Cassel D, Bigay J, Antonny B (2007) Two lipid-packing sensor motifs contribute to the

sensitivity of ArfGAP1 to membrane curvature. *Biochemistry* **46:** 1779–1790

Orci L, Palmer DJ, Amherdt M, Rothman JE (1993b) Coated vesicle assembly in the Golgi requires only coatomer and ARF proteins from the cytosol. *Nature* **364:** 732–734

Orci L, Palmer DJ, Ravazzola M, Perrelet A, Amherdt M, Rothman JE (1993a) Budding from Golgi membranes requires the coatomer complex of non-clathrin coat proteins. *Nature* **362:** 648–652

Poon PP, Cassel D, Spang A, Rotman M, Pick E, Singer RA, Johnston GC (1999) Retrograde transport from the yeast Golgi is mediated by two ARF GAP proteins with overlapping function. *EMBO J* **18:** 555–564

Presley JF, Ward TH, Pfeifer AC, Siggia ED, Phair RD, Lippincott-Schwartz J (2002) Dissection of COPI and Arf1 dynamics *in vivo* and role in Golgi membrane transport. *Nature* **417:** 187–193

Pucadyil TJ, Schmid SL (2009) Conserved functions of membrane active GTPases in coated vesicle formation. *Science* **325:** 1217–1220

Roux A, Cappello G, Cartaud J, Prost J, Goud B, Bassereau P (2002) A minimal system allowing tubulation with molecular motors pulling on giant liposomes. *Proc Natl Acad Sci USA* **99:** 5394–5399

Saitoh A, Shin HW, Yamada A, Waguri S, Nakayama K (2009) Three homologous ArfGAPs participate in coat protein I-mediated transport. *J Biol Chem* **284:** 13948–13957

Sato K, Nakano A (2005) Dissection of COPII subunit-cargo assembly and disassembly kinetics during Sar1p-GTP hydrolysis. *Nat Struct Mol Biol* **12:** 167–174

Schindler C, Rodriguez F, Poon PP, Singer RA, Johnston GC, Spang A (2009) The GAP domain and the SNARE, coatomer and cargo interaction region of the ArfGAP2/3 Glo3 are sufficient for Glo3 function. *Traffic* **10:** 1362–1375

Sorre B, Callan-Jones A, Manneville J-B, Nassoy P, Joanny J-F, Prost J, Goud B, Bassereau P (2009) Curvature-driven lipid sorting needs proximity to a demixing point and is aided by proteins. *Proc Natl Acad Sci USA* **106:** 5622–5626

Szafer E, Rotman M, Cassel D (2001) Regulation of GTP hydrolysis on ADP-ribosylation factor-1 at the Golgi membrane. *J Biol Chem* **276:** 47834–47839

Vasudevan C, Han W, Tan Y, Nie Y, Li D, Shome K, Watkins SC, Levitan ES, Romero G (1998) The distribution and translocation of the G protein ADP-ribosylation factor 1 in live cells is determined by its GTPase activity. *J Cell Sci* **111:** 1277–1285

Weimer C, Beck R, Eckert P, Reckmann I, Moelleken J, Brugger B, Wieland F (2008) Differential roles of ArfGAP1, ArfGAP2, and ArfGAP3 in COPI trafficking. *J Cell Biol* **183:** 725–735

Yang JS, Lee SY, Gao M, Bourgoin S, Randazzo PA, Premont RT, Hsu VW (2002) ARFGAP1 promotes the formation of COPI vesicles, suggesting function as a component of the coat. *J Cell Biol* **159:** 69–78